ARTICLE

Electrostatic Assembly of Sandwich-like Ag-C@ZnO-C@Ag-C Hybrid Hollow Microspheres with Excellent High-Rate Lithium Storage Properties

Qingshui Xie,[†] Yating Ma,[†] Xuanpeng Wang,[‡] Deqian Zeng,[†] Laisen Wang,[†] Liqiang Mai,[‡] and Dong-Liang Peng*,[†]
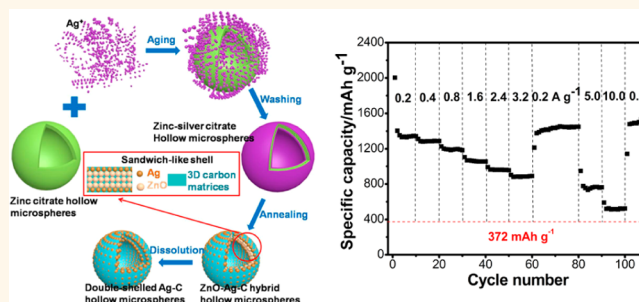
[†]Fujian Key Laboratory of Advanced Materials, Collaborative Innovation Center of Chemistry for Energy Materials, Department of Materials Science and Engineering, College of Materials, Xiamen University, Xiamen 361005, China
[‡]State Key Laboratory of Advanced Technology for Materials Synthesis and Processing, WUT-Harvard Joint Nano Key Laboratory, Wuhan University of Technology, Wuhan 430070, China

Ⓢ *Supporting Information*

ABSTRACT: Herein, we introduce a facile electrostatic attraction approach to produce zinc−silver citrate hollow microspheres, followed by thermal heating treatment in argon to ingeniously synthesize sandwich-like Ag-C@ZnO-C@Ag-C hybrid hollow microspheres. The 3D carbon conductive framework in the hybrids derives from the *in situ* carbonation of carboxylate acid groups in zinc−silver citrate hollow microspheres during heating treatment, and the continuous and homogeneous Ag nanoparticles on the outer and inner surfaces of hybrid hollow microspheres endow the shells with the sandwiched configuration (Ag-C@ZnO-C@Ag-C). When applied as the anode materials for lithium ion batteries, the fabricated hybrid hollow microspheres with sandwich-like shells reveal a very large reversible capacity of 1670 mAh g^{-1} after 200 cycles at a current density of 0.2 A g^{-1}. Even at the very large current densities of 1.6 and 10.0 A g^{-1}, the high specific capacities of about 1063 and 526 mAh g^{-1} can be retained, respectively. The greatly enhanced electrochemical properties of Ag-C@ZnO-C@Ag-C hybrid microspheres are attributed to their special structural features such as the hollow structures, the sandwich-like shells, and the nanometer-sized building blocks.

KEYWORDS: *zinc oxide, silver, sandwich-like shells, hybrid hollow microspheres, lithium storage properties*

R ecently, transition metal oxides have achieved enormous research interest for use as electrode materials in lithium ion batteries because of their high theoretical capacity, in an effort to substitute the conventional graphite anode, which illustrates the limited specific capacity of 372 mAh g^{-1}.[1−6] Among them, ZnO holds great promise as advanced anode materials due to its special merits as a rich resource and its diverse morphology, environmental friendliness, and high theoretical capacity (978 mAh g^{-1}), as well as the larger Li$^+$ diffusion coefficient than other transition metal oxides.[7,8] However, the pulverization of electrode materials and the poor electrochemical reaction kinetics caused respectively by the huge volume variation (over 228%) during the Li$^+$ insertion−extraction process and the intrinsic poor electronic conductivity of the ZnO anode would give rise to a greatly limited cyclability and rate capability. In addition, Zn nanocrystals formed during the discharging process would quickly migrate through the Li$_2$O matrices and then aggregate, thus leading to a severe capacity degradation. In this regard, despite ZnO's many merits, research focusing on lithium storage properties of materials has been rarely reported in the past decade.[9−12] How to effectively intensify the reversible capacity and cyclability of ZnO electrodes especially at a high rate still remains a great challenge.

Reducing the electrode materials to the nanoscale is a common strategy to enhance their rate capability by effectively shortening the Li$^+$ diffusion distances.[13−15] Unfortunately, the aggregation of nanosized active particles during cycling would cause serious performance degradation. Thus, the special robust

metal oxide micronanostructures (the micrometer-sized particles are made up of nanometer-sized building blocks) are regarded as one of the most ideal electrode materials since they not only possess the outstanding advantages of nanosized electrode materials but also can hinder the aggregation of electroactive nanoparticles during cycling to a large extent and ensure the good electrical properties of electrode materials.[16−18] On the other hand, the novel structural design of electrode materials has been proved to be anthor useful route to greatly strengthen their lithium storage properties by means of the well-orchestrated structural characteristics.[19−24] For example, Wang's group reported that thin triple-shell α-Fe₂O₃ hollow microspheres reveal higher reversible capacity than single-shell counterparts.[19] The enhanced electrochemical properties are mainly ascribed to the synergistic effect of the three shells in increasing mechanical strength of hollow microspheres as well as the inner void cavity to offer enough alleviating space for active materials during cycling.[25,26] Keeping such considerations in mind, it is of great significance to construct unique and novel micronanostructured metal oxide electrode materials through an ingenious structural design strategy, which are expected to reveal a remarkable high-rate lithium storage performance.

In this work, an innovative electrostatic attraction strategy is put forward to construct sandwich-like Ag-C@ZnO-C@Ag-C hybrid hollow microspheres that consist of numerous nanometer-sized building blocks. In these novel hybrid hollow microspheres, nanometer-sized subunits can shorten Li⁺ diffusion length and the 3D carbon conductive framework can enhance the electronic conductivity of the ZnO electrode, provide stable structural support, and hinder the aggregation of ZnO nanoparticles during cycling. The inner hollow space can effectively accommodate the huge volume variation of the ZnO material. More importantly, the continuous and uniform Ag nanoparticles on the outer and inner surfaces of hybrid hollow micropsheres (sandwich-like shells) not only can make electrons easily reach all the positions where lithium ion insertion takes place and provide more electron transport channels along with the small electron diffusion distance but also can effectively inhibit the large volume expansion of ZnO material. As a result, the novel sandwich-structured Ag-C@ZnO-C@Ag-C hybrid hollow microspheres show high reversible capacity, outstanding cyclability, and extraordinary rate capability when applied as the anode material for lithium ion batteries.

RESULTS AND DISCUSSION

The successful fabrication of sandwich-like Ag-C@ZnO-C@Ag-C hybrid hollow microspheres is schematically displayed in Figure 1, from which one can visibly find that this synthetic strategy comprises the initial aging treatment of zinc citrate hollow microspheres in silver nitrate solution at room temperature to achieve zinc−silver citrate hollow microsphere precursors, followed by the thermal annealing treatment in argon, which is simple and efficient. As manifested in Figure S1, the initial zinc citrate hollow microspheres possess relative loose and rough surfaces. The positive silver ions would adsorb on the outer and inner surfaces of zinc citrate hollow microspheres during the aging process because of the electrostatic interaction with the negative carboxylate acid groups (−COO⁻) and hydroxide groups (−OH) in zinc citrate, causing the formation of zinc−silver citrate hollow microspheres.[28,29] During the annealing process, the carboxylate acid
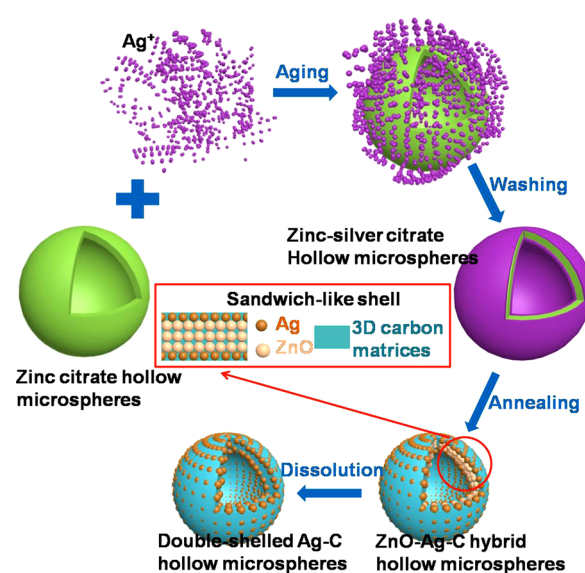

Figure 1. Schematic illustration of the facile synthesis of sandwich-like Ag-C@ZnO-C@Ag-C hybrid hollow microspheres.

groups in the zinc−silver citrate not only function as the *in situ* carbon sources to prepare the 3D carbon conductive framework throughout the whole hollow microspheres but also act as anchors to restrict the growth and aggregation of ZnO and Ag nanoparticles, thus benefiting the uniform distribution of small Ag nanoparticles to form continuous Ag layers on the outer and inner surfaces of hybrid hollow microspheres. In order to get further insight into the structures of hybrids, the harvested ZnO/Ag/C hybrid hollow microspheres are added into NaOH solution to selectively dissolve the high content of ZnO, finally leading to the generation of the double-shelled Ag−C hollow microspheres.

The SEM and TEM images (Figure S2) manifest that the achieved zinc−silver citrate precursor consists of a great deal of dispersed hollow microspheres with a relatively rough surface and about 1.7 μm in diameter. The energy dispersive spectroscopy (EDS) measurement is in support of the successful adsorption of silver ions on the surfaces of zinc citrate hollow microspheres with a Ag/Zn molar ratio of approximate 0.231 (Figure S3). The X-ray diffraction (XRD) pattern (Figure 2a) indicates the main amorphous characteristic of the obtained zinc−silver citrate hollow microspheres, in good correspondence with the initial zinc citrate hollow microspheres.[27]

By heating treatment of zinc−silver citrate hollow microspheres in argon, ZnO/Ag/C hybrids can be fabricated. Figure 2b demonstrates the XRD pattern of the annealed product, wherein the diffraction peaks can be assigned to hexagonal ZnO (JCPDS card No. 36-1451) and cubic Ag (JCPDS card No. 04-0783), respectively. The *in situ* carbonation of carboxylate acid groups in the precursor during heating treatment would form a 3D carbon conductive framework throughout the whole hollow microspheres, and no diffraction peaks originating from carbon can be observed, indicative of the amorphous feature of such derived carbon. Of particular note, the 3D carbon conductive framework would effectively restrict the growth and aggregation of ZnO and Ag nanoparticles during annealing treatment, giving rise to the small crystallite sizes and consequently accounting for the broadening diffraction peaks of ZnO and Ag. In order to elucidate this point more clearly, zinc−silver citrate
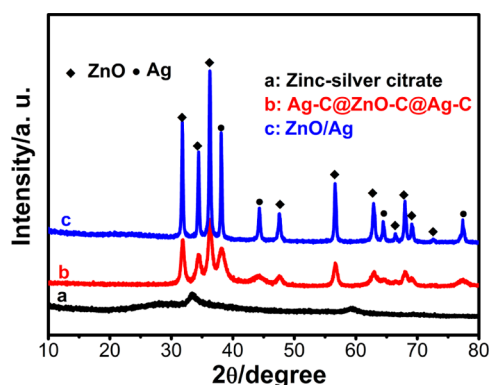
Figure 2. XRD patterns of Ag-C@ZnO-C@Ag-C, ZnO/Ag, and zinc−silver citrate hollow microspheres.

hollow microspheres are annealed in air under the same temperature to completely remove carbon. As expected, the sharper and stronger XRD diffraction peaks imply the larger crystallite sizes of ZnO and Ag in ZnO/Ag hybrids (Figure 2c). This behavior would be further confirmed from the SEM investigation shown below.

Figure 3 suggests the success in preparation of sandwich-like Ag-C@ZnO-C@Ag-C hybrid hollow microspheres. Representative SEM images (Figure 3a,b) demonstrate that the dispersed hybrid microspheres about 1.15 μm in diameter are made up of many nanometer-sized building blocks, in good

agreement with the above XRD result (Figure 2b). The inner hollow space of the hybrid microsphere can be observed from the broken particle shown in Figure 3c and TEM observations shown in Figure 3d,e. The contents of Ag, ZnO, and C in the hybrid hollow microspheres are respectively about 21.5, 72.5, and 6.0 wt %, acquired from the ICP measurement. The two lattice fringes with spacing distances of 0.28 and 0.24 nm in the HRTEM image (Figure 3f) are assigned to the (100) plane of hexagonal ZnO and the (111) plane of cubic Ag, respectively. The SAED pattern (Figure 3g) indicates the polycrystalline characteristic of the hybrid hollow microspheres. Scanning TEM (STEM) micrograph and the dot-mapping images (Figure 3h,i) manifest that all the elements are homogeneously distributed within the whole hollow microsphere and no large Ag aggregates can be seen. The TG measurement suggests that the carbon content in the hybrid hollow microspheres is about 5.80% (Figure S4), which is consonant with the above ICP evaluation.

In order to further elucidate the shell structure of ZnO/Ag/C hybrid hollow microspheres, the produced hybrid hollow microspheres are added into a NaOH solution to selectively remove ZnO. Of interest, double-shelled Ag−C hollow microspheres could be acquired (Figure 4a−c and Figure S5). The HRTEM image (Figure 4d) derived from the square region in Figure 4c clearly reveals that the Ag nanoparticles are completely embedded into the amorphous carbon matrix. The SAED pattern evidences the polycrystalline nature of the double-shelled Ag−C hollow microspheres (Figure 4e). STEM
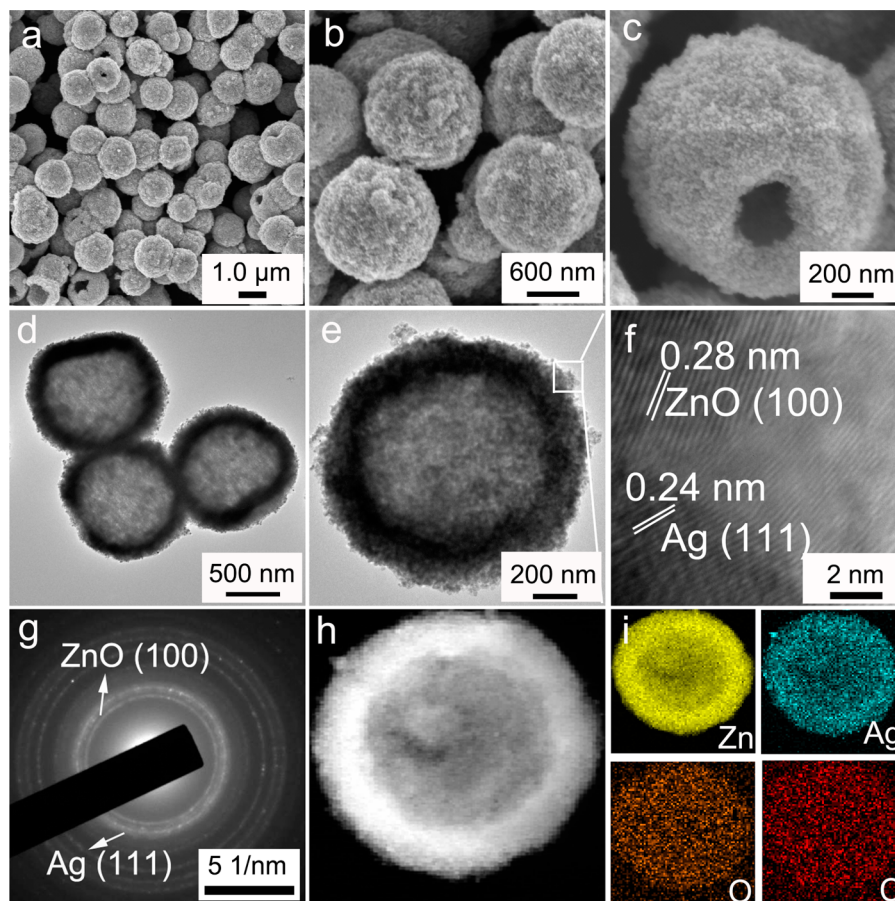

Figure 3. SEM (a−c), TEM (d, e) and HRTEM (f) micrographs of sandwich-like Ag-C@ZnO-C@Ag-C hybrid hollow microspheres. SAED pattern (g), STEM image (h), and the corresponding dot-mapping images (i) of hybrid hollow microspheres.
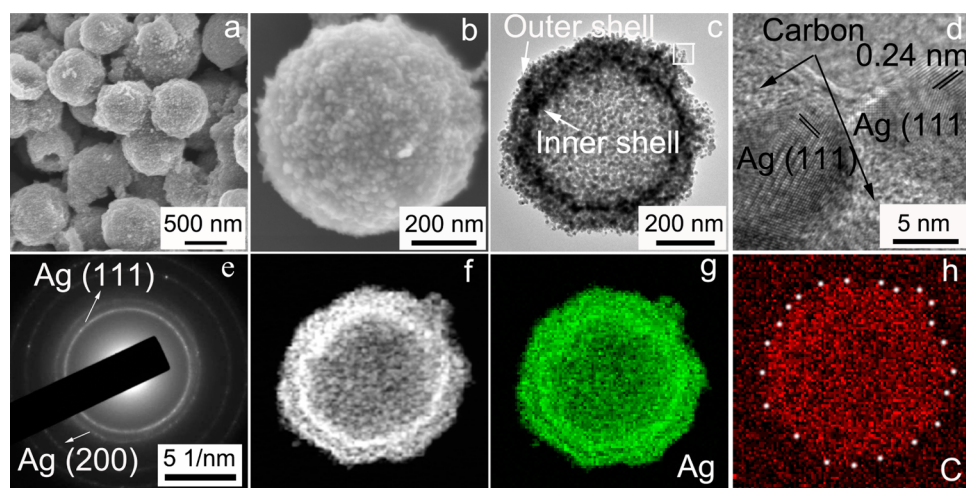
Figure 4. SEM (a, b), TEM (c), and HRTEM (d) images of double-shelled Ag−C hollow microspheres obtained by selectively dissolving ZnO in ZnO/Ag/C hybrid hollow microspheres. The SAED pattern (e), STEM image (f), and corresponding element mappings of Ag (g) and C (h) of double-shelled Ag−C hollow microspheres.
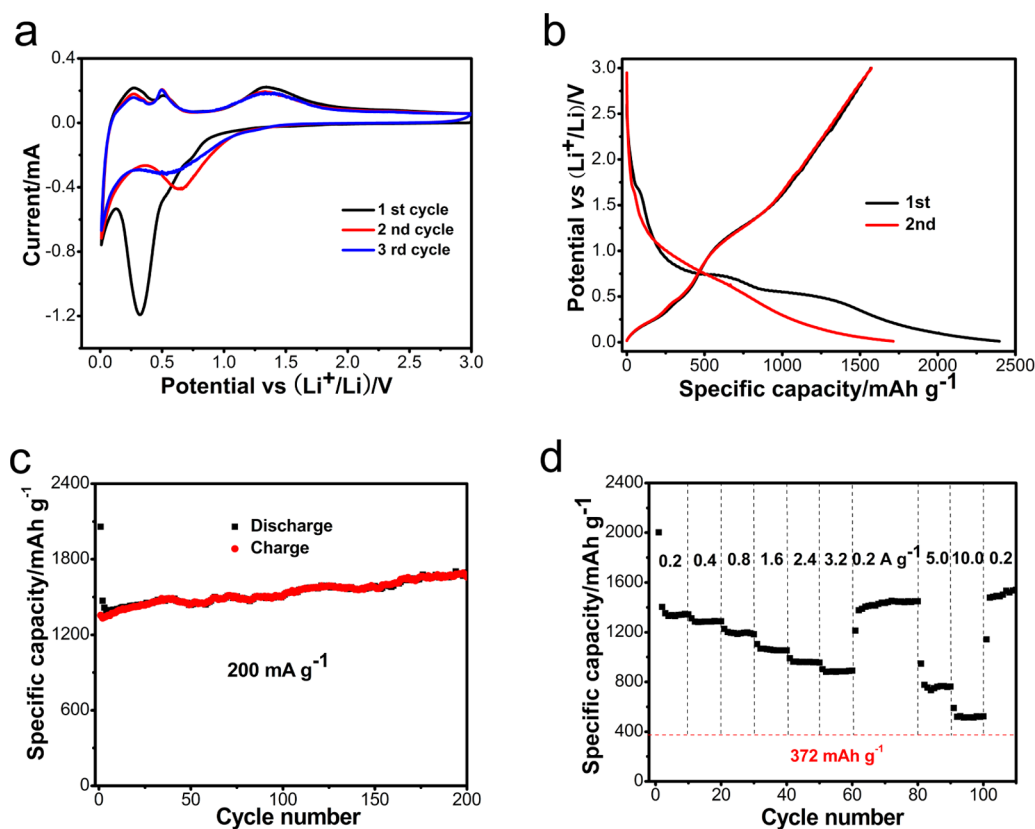

Figure 5. CV curves at 0.1 mV s^{-1} between 0.01 and 3.0 V (a), galvanostatic discharge−charge profiles (b), cycling performances at 200 mA g^{-1} (c), and rate capability at various current densities (d) of sandwich-like Ag-C@ZnO-C@Ag-C hybrid hollow microspheres.

micrograph and the dot-mapping images (Figure 4f−h) evidence the uniform distributions of Ag nanoparticles on the outer and inner shells of hollow microspheres and the 3D carbon conductive framework throughout the whole hollow microspheres. From all the above SEM and TEM characterizations and analysis, the sandwich-like shells (Ag-C@ZnO-C@Ag-C) of ZnO/Ag/C hybrid hollow microspheres can be visualized vividly.

By contrast, the SEM and TEM images of ZnO/Ag hybrids prepared through heating treatment of zinc−silver citrate hollow microspheres in air under the same temperature are shown in Figure S6. It can be easily found that ZnO/Ag hybrid hollow microspheres are made up of the larger ZnO and Ag nanoparticles in this condition, which is in good agreement with their above XRD result (Figure 2c). In the absence of the anchor effect of a 3D carbon framework, ZnO and Ag nanoparticles would move more easily and grow quickly by virtue of the decreased surface energy during the heating process, resulting in the formation of the larger ZnO and Ag nanoparticles and the uneven spatial distribution of Ag on the

outer and inner surfaces of the ZnO hollow microspheres (Figure S6g−i). Accordingly, it can be reasonably concluded that the carboxylate acid groups in zinc−silver citrate precursor play a critical role in the synthesis of sandwich-like Ag-C@ZnO-C@Ag-C hybrid hollow microspheres, which not only function as the *in situ* carbon source to prepare 3D carbon conductive framework throughout the whole hollow microspheres but also act as anchors to restrict the growth and aggregation of ZnO and Ag nanoparticles during the heating process, leading to the generation of sandwich-structured shells.

N$_2$ adsorption−desorption isotherm characterizations exhibited in Figure S7 suggest the presence of mesopores in the sandwich-like Ag-C@ZnO-C@Ag-C hybrid hollow microspheres and the largest Brunauer−Emmett−Teller (BET) specific surface area of 98.0 m^2 g^{-1}. The BET surface areas of ZnO/Ag hybrid hollow microspheres and single ZnO hollow microspheres gained by direct calcination of the initial zinc citrate hollow microspheres at 500 °C in air are 15.2 and 14.7 m^2 g^{-1}, respectively.

Figure 5a is the first three cyclic votammograms (CVs) of the anode assembled by sandwich-like Ag-C@ZnO-C@Ag-C hybrid hollow microspheres at a scan rate of 0.1 mV s^{-1} between 0.01 and 3.0 V. Two small shoulders around 0.74 and 0.53 V indicated by black arrows can be discerned carefully during the first cathodic scan. The former shoulder presumably originates from the decomposition of the electrolyte to generate a solid electrolyte interphase (SEI) layer.[30,31] It is well established that the conversion reaction between ZnO and Li$^+$ to form Zn and Li$_2$O and the subsequent alloying reaction between Zn and Li$^+$ to generate Li$_x$Zn alloys generally take place at about 0.5 and 0.25 V, respectively.[8] In our work, the reduction peaks related to the above-mentioned two electrochemical reactions overlap partially in the same potential range, leading to a broad and strong reduction peak centered at 0.32 V and a small shoulder near 0.53 V. This phomemon is common for many other ZnO-based anodes, and the position of this broad reduction peak relates to the morphology and composition of electrode materials.[11,32,33] The peak located at 0.01 V corresponds to the intercalation of lithium ion into carbon.[34] The following anodic scan shows three oxidation peaks located at 0.26, 0.50, and 1.33 V. The peak around 0.26 V is associated with the lithium ions' deintercalation from carbon and the initial-step dealloying reaction of Li$_x$Zn alloys.[11,35] These two electrochemical reactions take place at very close potential, resulting in only one broad oxidation peak. The peak located at 0.50 V relates to the further dealloying reaction of Li$_x$Zn alloys to form Zn metal, and the peak near 1.33 V is caused by the oxidation of Zn to generate ZnO.[36] No redox peaks resulting from Ag in the CV curve can be observed because Ag functions only as the additive to increase the electronic conductivity of electrode materials.[37,38] There is little change in the peak position and shape in the following cathodic/anodic scanning curves, suggesting that the electrode reactions take place reversibility.

The potential *versus* capacity curves of sandwich-like Ag-C@ZnO-C@Ag-C hybrid hollow microspheres at 100 mA g^{-1} within 0.01−3.0 V are exhibited in Figure 5b. Two pronounced plateaus around 0.74 and 0.54 V in the first lithiation process respectively stem from the decomposition of the electrolyte to generate the SEI layer and the reduction of ZnO.[11,39] A weak and inconspicuous plateau located at 0.25 V can be attentively distinguished, being attributed to the subsequent alloying reactions between Zn and Li$^+$ to form Li$_x$Zn alloys. There are three poorly defined plateaus located at 0.29, 0.56, and 1.33 V in the first delithiation profile, originating from the multistep dealloying reactions of Li$_x$Zn alloys and the regeneration of ZnO, respectively. The results are in good accordance with the above CV characterization. The sandwich-like Ag-C@ZnO-C@Ag-C hybrid hollow microspheres display initial discharge/charge capacities of about 2396/1569 mAh g^{-1}. The achieved Coulombic efficiency is about 65.4%, which is higher than the ZnO/Ag hybrid hollow microspheres (49.0%, Figure S8a) and yolk−shell ZnO/C hollow microspheres (48.8%) reported in our earlier work.[10] The irreversible capacity loss during the first cycle may be caused by the formation of the SEI layer derived from the decomposition of the electrolyte.[19,40] The uniform decoration of Ag in the active materials is helpful to prohibit the decomposition of solvent and benefits the generation of a stable and thin SEI layer on the surfaces of the electrode materials, which probably accounts for the enhanced initial Coulombic efficiency of sandwich-like Ag-C@ZnO-C@Ag-C hybrid hollow microspheres.[41,42]

The cyclability of sandwich-like Ag-C@ZnO-C@Ag-C hybrid hollow microspheres is tested at a current density of 200 mA g^{-1} within 0.01−3.0 V, and the corresponding result is depicted in Figure 5c. Interestingly, the reversible capacity of hybrid hollow microspheres continuously increases with cycle number. After 200 cycles, a very large discharge capacity of 1670 mAh g^{-1} can be retained, demonstrating very high reversible capacity and excellent cycling stability of the sandwich-like Ag-C@ZnO-C@Ag-C hybrid hollow microspheres. The achieved reversible capacity of hybrid hollow microspheres is higher than that of the theoretical capacity for ZnO (978 mAh g^{-1}). The Coulombic efficiency of sandwich-like Ag-C@ZnO-C@Ag-C hybrid hollow microspheres maintains a stability of over 99.0% from the tenth cycle onward, indicating that the electrochemical reactions are highly reversible. As is well-known, the polymeric gel-like films formed on the electroactive particles would experience reversible growth and decomposition during the Li$^+$ insertion−extraction process, which would consume a certain amount of lithium ions to contribute to extra reversible capacity.[43,44] In addition, the electrode materials are taken out from the cell after 200 cycles and washed with methyl carbonate to remove the residual electrolyte for *ex situ* XRD measurement. As shown in Figure S9, the diffraction peaks originating from Li$_2$CO$_3$ and Li$_2$O can be carefully distinguished. Combining the above Coulombic efficiency analysis, the *ex situ* XRD investigation, and the previous relative literature, it can be reasonably affirmed that the excess reversible capacity of the sandwich-like Ag-C@ZnO-C@Ag-C hybrid hollow microspheres electrode over its theoretical capacity value is caused by the reversible formation of polymeric gel-like films during cycling.[19,36,45,46] More studies should be carried out in the future in order to better understand the mechanism of the enhanced lithium storage properties. It is well accepted that the serious capacity degradation of ZnO electrodes especially at high rate greatly restricts their potential application in lithium ion batteries. In this context, the produced sandwich-like Ag-C@ZnO-C@Ag-C hybrid hollow microsphere electrode is further measured at a large current density of 1000 mA g^{-1} within 0.01−3.0 V (Figure S10). Impressively, the discharge capacities of Ag-C@ZnO-C@Ag-C hybrid hollow microspheres remain stable at nearly 1250 mAh g^{-1} from the fourth cycle onward, indicating the exceptional cycling stability of hybrid hollow microspheres even at a large

rate of 1000 mA g^{-1}. Figure S8b reveals the lithium storage properties of ZnO/Ag and single ZnO hollow microspheres. In sharp contrast, both ZnO/Ag and single ZnO hollow microspheres demonstrate serious capacity degradation even at a low current density of 100 mA g^{-1}. In our earlier work, hierarchical ZnO-Ag-C composite porous microspheres were fabricated, which delivered a reversible capacity of 729 mA g^{-1} at 100 mA g^{-1} after 200 cycles.[47] Obviously, sandwich-like Ag-C@ZnO-C@Ag-C hybrid hollow microspheres depict the highest specific capacity and best cycling stability.

Similar to Li$^+$ insertion−extraction, the transport of electrons in electrode materials also exerts a significant effect on their electrochemical properties.[48−50] ZnO is a semiconductor and its large resistance originating from the poor electronic conductivity would suppress its lithium storage properties to a large extent. In order to clearly illustrate the special structural advantages of the sandwich-like Ag-C@ZnO-C@Ag-C hybrid hollow microsphere, the schematic illustrations of the electron transport process during cycling for various ZnO-based hybrid microspheres are shown in Figure 6 and Figure S11. In the
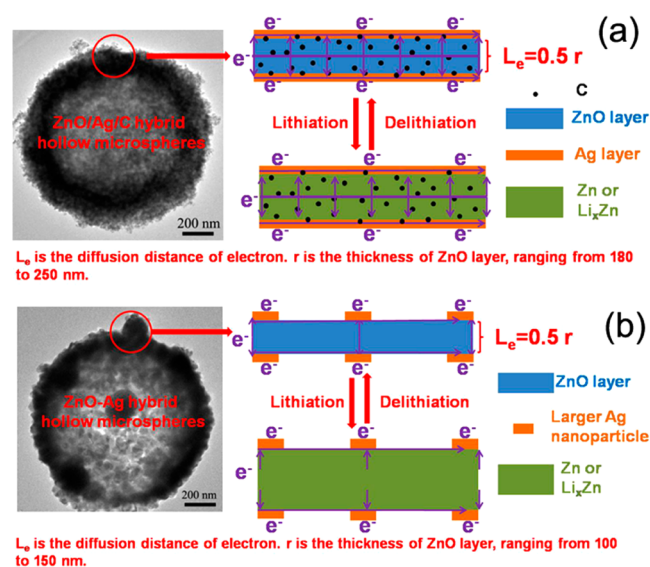

Figure 6. Schematic illustrations of electron transport process during cycling for sandwich-like Ag-C@ZnO-C@Ag-C hybrid hollow microspheres (a) and ZnO/Ag hybrid hollow microspheres (b).

sandwich-like Ag-C@ZnO-C@Ag-C hybrid hollow microspheres, both sides of the ZnO layer are covered with continuous and uniform Ag layers due to their unique

sandwich-constructed shells (the homogeneously dispersed small Ag nanoparticles on the outer and inner surfaces of hollow microspheres can be deemed as two continuous and uniform Ag layers). This feature can not only provide more electron transport channels but also offer the significantly decreased diffusion distance of electrons (L_e), comparable to the half-thickness of the ZnO layer (180−250 nm). However, Ag nanoparticles only exist on the outer surfaces of ZnO-Ag-C composite porous microspheres. Namely, there is only one side of the ZnO materials in contact with the Ag nanoparticles, and the relatively low content of Ag (1.03 wt %) may be not enough to form a continuous Ag layer. Consequently, ZnO-Ag-C composite porous microspheres possess fewer electron transport channels and far bigger L_e (1300−1600 nm). With respect to ZnO/Ag hybrid hollow microspheres and yolk−shell ZnO-C microspheres, no extra electron transport channels (continuous and uniform Ag layers) are formed; thus the electronic conductivity of electrode materials cannot be enhanced effectively. In addition, the sandwich-constructed shells of Ag-C@ZnO-C@Ag-C hybrid hollow microspheres can prohibit the volume expansion of ZnO active materials during the lithiation/delithiation process more effectively, which is conducive to maintain the integrity of the electrode. Three cells assembled respectively by Ag-C@ZnO-C@Ag-C, ZnO/Ag, and ZnO hollow microspheres after 100 cycles are dismantled for SEM measurement (Figure S12). As expected, the microspherical morphology of Ag-C@ZnO-C@Ag-C hybrids indicated by arrows is basically maintained after cycling, while the hollow structures of ZnO/Ag and ZnO microspheres are destroyed and cracked, verifying the better structural stability of Ag-C@ZnO-C@Ag-C hybrid hollow microspheres. Thus, it can be concluded that the sandwich-constructed shells of Ag-C@ZnO-C@Ag-C hybrid hollow microspheres play a critical role in their high reversible capacity and outstanding cyclability, and these results also emphasize the importance of ingenious design and controllable synthesis of electrode materials.

Figure 5d manifests the rate performance of sandwich-like Ag-C@ZnO-C@Ag-C hybrid hollow microsphere. The average reversible capacities of about 1412, 1288, 1196, 1063, 963, 886, and 778 mAh g^{-1} can be achieved at current densities of 200, 400, 800, 1600, 2400, 3200, and 5000 mA g^{-1}, respectively. Remarkably, even at the very large current density of 10 000 mA g^{-1}, a high specific capacity of 526 mAh g^{-1} can be retained, which is still higher than the theoretical capacity of a commercial graphite electrode (372 mAh g^{-1}). Most importantly, the reversible capacity is capable of returning to the original value (more than 1471 mAh g^{-1}) when the current

Table 1. Rate Capabilities of Various ZnO-Based Electrodes in Lithium Ion Batteries

materials	morphology	reversible capacity (mAh g^{-1})	current density (A g^{-1})	ref
ZnO-C	quantum dots	400	3.75	12
ZnO-C	nanoparticles	497	1.0	53
ZnO-C	yolk−shell microspheres	212	1.0	10
ZnO-graphene	nanocomposites	415	1.0	11
ZnO-graphene	nanocomposites	<400	2.0	34
ZnO-graphene	nanocomposites	400	1.0	39
ZnO-NiO	porous hybrid nanofibers	707	3.2	36
ZnO-Mn$_3$O$_4$	yolk−shell microspheres	460	3.0	52
ZnO-ZnFe$_2$O$_4$	submicrocubes	667	2.0	51
Ag-C@ZnO-C@Ag-C	sandwich-like hybrid hollow microspheres	1196/1063/778/526	0.8/1.6/5.0/10.0	our work

density is restored to the initial 200 mA g^{-1}, indicating an exceptional rate performance and reversibility of a sandwich-structured hybrid hollow microsphere electrode. Compared to ZnO/Ag and single ZnO hollow microspheres, Ag-C@ZnO-C@Ag-C hybrid hollow microspheres undoubtedly depict the significantly strengthened rate capability (Figure S8c). To our knowledge, this is the best high-rate performance at such high current rate among other ZnO-based electrodes reported previously (Table 1).[10−12,34,36,39,51−53] For instance, Park's group recently reported the successful fabrication of carbon-coated ZnO quantum dots that delivered a specific capacity of about 400 mAh g^{-1} at a current density of 3.75 A g^{-1}.[12] Hierarchical mesoporous ZnO/ZnFe$_2$O$_4$ submicrocubes prepared by Hou et al. exhibited reversible capacities of about 728 and 667 mAh g^{-1} at current densities of 1000 and 2000 mA g^{-1}, respectively.[51]

The remarkable electrochemical properties of the produced sandwich-like Ag-C@ZnO-C@Ag-C hybrid hollow microspheres are attributed to their special structural features. First of all, the hollow interiors of hybrid microspheres are helpful in buffering the dramatic volume change during the lithiation/delithiation process by offering extra void space, consequently benefiting cyclability.[26,54] Additionally, more electroactive sites can be provided due to the largest specific surface area of Ag-C@ZnO-C@Ag-C hybrid hollow microspheres compared to ZnO/Ag and single ZnO hollow microspheres, which can improve the specific capacity of the electrode. Second, the obtained Ag-C@ZnO-C@Ag-C hybrid hollow microspheres are composed of numerous small nanometer-sized subunits. Such secondary micronanostructures not only have the merits of the shortened lithium ion diffusion distance but also can impede the aggregation of electroactive nanoparticles to some extent during cycling and ensure good electrical properties of electrode materials.[20,55] Third, the 3D carbon conductive framework throughout the whole hollow microspheres can enhance the structural stability of the electrode, restrict the self-aggregation of ZnO nanoparticles during cycling, and strengthen the electronic conductivity of active materials, leading to enhanced cyclability and rate capability.[56] Finally, the elaborately constructed sandwich-like shells of Ag-C@ZnO-C@Ag-C hybrid hollow microspheres can provide more electron transport channels and a shortened diffusion distance of the electron, giving rise to a significantly enhanced electronic conductivity. This behavior has been identified from the electrochemical impedance spectroscopy (EIS) investigations displayed in Figure S13. The increased electronic conductivity can effectively enhance the electrochemical reaction kinetics of electrode materials and thus benefit the rate performance. Furthermore, the sandwich-like shells can hinder the large volume expansion of ZnO active materials during the lithiation/delithiation process to some extent, which is conducive to maintain the integrity of the electrode. By combining all of the above advantages, sandwich-like Ag-C@ZnO-C@Ag-C hybrid hollow microspheres demonstrate the excellent electrochemical properties of high specific capacity, outstanding cyclability, and exceptional rate capability when applied as the anode material in lithium ion batteries.

CONCLUSIONS

In summary, we have put forward a facile electrostatic attraction approach to fabricate sandwich-like Ag-C@ZnO-C@Ag-C hybrid hollow microspheres by annealing treatment of zinc−silver citrate hollow microspheres in argon. The carboxylate acid groups in the zinc−silver citrate precursor not only function as the in situ carbon source to prepare a 3D carbon conductive framework throughout the whole hollow microspheres but also act as anchors to restrict the growth and aggregation of ZnO and Ag nanoparticles during thermal treatment. The unique structural characteristics of the produced Ag-C@ZnO-C@Ag-C hybrids including the hollow construction of microspheres, the large specific surface area, nanometer-sized subunits, the robust sandwich-structured shells, and the 3D carbon conductive framework endow them with excellent electrochemical properties of high specific capacity, remarkable cyclability, and outstanding rate performance. This work may emphasize the significance of the ingenious design and controllable synthesis of anode materials for the development of high-rate performance lithium ion batteries.

METHODS

Synthesis. Typically, zinc citrate hollow microspheres (0.10 g) that were preproduced based on our earlier paper[27] were dispersed into 50 mL of silver nitrate solution (0.005 mol) to form a uniform suspension under ultrasonication, followed by an aging treatment at room temperature for 1 h. Then, the white zinc−silver citrate precipitant was centrifuged and purged with deionized water several times. Sandwich-like Ag-C@ZnO-C@Ag-C hybrid hollow microspheres could be obtained by calcination of the above achieved precipitant at 500 °C for 2 h in argon. In order to get further insight into the structure of the hybrids, the obtained Ag-C@ZnO-C@Ag-C hybrid hollow microspheres were added into 25 mL of NaOH solution (4 M) and stirred magnetically for 5 h to selectively dissolve ZnO.

Characterizations. The obtained samples are subjected to detailed investigations to identify their phases, morphologies, structures, BET specific surface areas, and carbon content using a PANalytical X'pert PRO X-ray diffractometer (Cu Kα radiation 40 kV, 30 mA), scanning electron microscopy (SEM, Hitachi SU-70), transmission electron microscopy (TEM, JEM-2100, 200 kV), a TriStar 3020 system, and an SDT-Q600 thermal analyzer, respectively.

Electrochemical Measurements. The lithium storage properties of the achieved products were tested by manufacturing 2025 coin cells in an argon-filled glovebox. A metal lithium disk and Celgard 2300 serve as the counter and reference electrodes and the separator, respectively. The electroactive particles (hybrid hollow microspheres), acetylene black, and poly(vinyl difluoride) with a 7:2:1 weight ratio are dispersed in N-methylpyrrolidone to generate a uniform suspension. Then the suspension is coated on a copper foil (d = 1.6 cm) to fabricate the working electrode. The coating density of the active materials is about 1 mg cm^{-2}. One molar LiPF$_6$ in a mixed solution of ethylene carbonate and diethyl carbonate (1:1 in volume) functions as the electrolyte. Cyclic voltammetry and electrochemical impedance spectroscopy tests were implemented by employing an Autolab electrochemical workstation. The cycling and rate performances of the electrodes were recorded by applying Neware battery testers. Because Ag is inactive to lithium ion, the specific capacity of the electrode is calculated according to the mass of ZnO and carbon.

ASSOCIATED CONTENT

Ⓢ **Supporting Information**

The Supporting Information is available free of charge on the ACS Publications website at DOI: 10.1021/acsnano.5b06650.

> Additional figures including SEM/TEM images, EDS spectra, TGA curve, N$_2$ adsorption−desorption isotherms, and the relative electrochemical properties of the initial zinc citrate, zinc−silver citrate precursor, ZnO/Ag, and Ag-C@ZnO-C@Ag-C hollow microspheres (PDF)

AUTHOR INFORMATION

Corresponding Author
*E-mail: dlpeng@xmu.edu.cn.

Notes
The authors declare no competing financial interest.

ACKNOWLEDGMENTS

REFERENCES

(1) Liang, J.; Yu, X. Y.; Zhou, H.; Wu, H. B.; Ding, S.; Lou, X. W. Bowl-Like SnO_2@Carbon Hollow Particles as an Advanced Anode Material for Lithium-Ion Batteries. *Angew. Chem., Int. Ed.* **2014**, *53*, 12803−12807.

(2) He, C.; Wu, S.; Zhao, N.; Shi, C.; Liu, E.; Li, J. Carbon-Encapsulated Fe_3O_4 Nanoparticles as a High-Rate Lithium Ion Battery Anode Material. *ACS Nano* **2013**, *7*, 4459−4469.

(3) Jiang, H.; Hu, Y.; Guo, S.; Yan, C.; Lee, P. S.; Li, C. Rational Design of MnO/Carbon Nanopeapods with Internal Void Space for High-Rate and Long-Life Li-Ion Batteries. *ACS Nano* **2014**, *8*, 6038−6046.

(4) Wu, Z. S.; Ren, W.; Wen, L.; Gao, L.; Zhao, J.; Chen, Z.; Zhou, G.; Li, F.; Cheng, H. M. Graphene Anchored with Co_3O_4 Nanoparticles as Anode of Lithium Ion Batteries with Enhanced Reversible Capacity and Cyclic Performance. *ACS Nano* **2010**, *4*, 3187−3194.

(5) Wang, Z.; Luan, D.; Madhavi, S.; Hu, Y.; Lou, X. W. Assembling Carbon-Coated α-Fe_2O_3 Hollow Nanohorns on the CNT Backbone for Superior Lithium Storage Capability. *Energy Environ. Sci.* **2012**, *5*, 5252−5256.

(6) Huang, X.-L.; Wang, R.-Z.; Xu, D.; Wang, Z.-L.; Wang, H.-G.; Xu, J.-J.; Wu, Z.; Liu, Q.-C.; Zhang, Y.; Zhang, X.-B. Homogeneous CoO on Graphene for Binder-Free and Ultralong-Life Lithium Ion Batteries. *Adv. Funct. Mater.* **2013**, *23*, 4345−4353.

(7) Ren, Z.; Wang, Z.; Chen, C.; Wang, J.; Fu, X.; Fan, C.; Qian, G. Preparation of Carbon-Encapsulated ZnO Tetrahedron as an Anode Material for Ultralong Cycle Life Performance Lithium-Ion Batteries. *Electrochim. Acta* **2014**, *146*, 52−59.

(8) Zhang, G.; Hou, S.; Zhang, H.; Zeng, W.; Yan, F.; Li, C. C.; Duan, H. High-Performance and Ultra-Stable Lithium-Ion Batteries Based on MOF-Derived ZnO@ZnO Quantum Dots/C Core-Shell Nanorod Arrays on a Carbon Cloth Anode. *Adv. Mater.* **2015**, *27*, 2400−2405.

(9) Huang, X.; Xia, X.; Yuan, Y.; Zhou, F. Porous ZnO Nanosheets Grown on Copper Substrates as Anodes for Lithium Ion Batteries. *Electrochim. Acta* **2011**, *56*, 4960−4965.

(10) Xie, Q.; Zhang, X.; Wu, X.; Wu, H.; Liu, X.; Yue, G.; Yang, Y.; Peng, D.-L. Yolk-Shell ZnO-C Microspheres with Enhanced Electrochemical Performance as Anode Material for Lithium Ion Batteries. *Electrochim. Acta* **2014**, *125*, 659−665.

(11) Yu, M.; Wang, A.; Wang, Y.; Li, C.; Shi, G. An Alumina Stabilized ZnO-Graphene Anode for Lithium Ion Batteries *via* Atomic Layer Deposition. *Nanoscale* **2014**, *6*, 11419−11424.

(12) Yang, S. J.; Nam, S.; Kim, T.; Im, J. H.; Jung, H.; Kang, J. H.; Wi, S.; Park, B.; Park, C. R. Preparation and Exceptional Lithium Anodic Performance of Porous Carbon-Coated ZnO Quantum Dots Derived from a Metal-Organic Framework. *J. Am. Chem. Soc.* **2013**, *135*, 7394−7397.

(13) Bruce, P. G.; Scrosati, B.; Tarascon, J. M. Nanomaterials for Rechargeable Lithium Batteries. *Angew. Chem., Int. Ed.* **2008**, *47*, 2930−2946.

(14) Zhou, L.; Zhao, D. Y.; Lou, X. W. $LiNi_{0.5}Mn_{1.5}O_4$ Hollow Structures as High-Performance Cathodes for Lithium-Ion Batteries. *Angew. Chem.* **2012**, *124*, 243−245.

(15) Jiang, C. H.; Hosono, E.; Zhou, H. S. Nanomaterials for Lithium Ion Batteries. *Nano Today* **2006**, *1*, 28−33.

(16) Yuan, C. Z.; Wu, H. B.; Xie, Y.; Lou, X. W. Mixed Transition-Metal Oxides: Design, Synthesis, and Energy-Related Applications. *Angew. Chem., Int. Ed.* **2014**, *53*, 1488−1504.

(17) Li, Z.; Li, B.; Yin, L.; Qi, Y. Prussion Blue-Supported Annealing Chemical Reaction Route Synthesized Double-Shelled Fe_2O_3/Co_3O_4 Hollow Microcubes as Anode Materials for Lithium-Ion Battery. *ACS Appl. Mater. Interfaces* **2014**, *6*, 8098−8107.

(18) Wu, R.; Qian, X.; Zhou, K.; Wei, J.; Lou, J.; Ajayan, P. M. Porous Spinel $Zn_xCo_{3-x}O_4$ Hollow Polyhedra Templated for High-Rate Lithium-Ion Batteries. *ACS Nano* **2014**, *8*, 6297−6303.

(19) Xu, S.; Hessel, C. M.; Ren, H.; Yu, R.; Jin, Q.; Yang, M.; Zhao, H.; Wang, D. α-Fe_2O_3 Multi-Shelled Hollow Microspheres for Lithium Ion Battery Anodes with Superior Capacity and Charge Retention. *Energy Environ. Sci.* **2014**, *7*, 632−637.

(20) Hu, L.; Zhong, H.; Zheng, X.; Huang, Y.; Zhang, P.; Chen, Q. $CoMn_2O_4$ Spinel Hierarchical Microspheres Assembled with Porous Nanosheets as Stable Anodes for Lithium-ion Batteries. *Sci. Rep.* **2012**, *2*, 986−993.

(21) Sun, X.; Yan, C.; Chen, Y.; Si, W.; Deng, J.; Oswald, S.; Liu, L.; Schmidt, O. G. Three-Dimensionally Curved NiO Nanomembranes as Ultrahigh Rate Capability Anodes for Li-Ion Batteries with Long Cycle Life Times. *Adv. Energy Mater.* **2014**, *4*, 1300912.

(22) Wang, H.; Ma, D.; Huang, X.; Huang, Y.; Zhang, X. General and Controllable Synthesis Strategy of Metal Oxide/TiO_2 Hierarchical Heterostructures with Improved Lithium-Ion Battery Performance. *Sci. Rep.* **2012**, *2*, 701−708.

(23) Li, S.; Niu, J.; Zhao, Y. C.; So, K. P.; Wang, C.; Wang, C. A.; Li, J. High-Rate Aluminium Yolk-Shell Nanoparticle Anode for Li-Ion Battery with Long Cycle Life and Ultrahigh Capacity. *Nat. Commun.* **2015**, *6*, 7872−7278.

(24) Ma, D.-L.; Cao, Z.-Y.; Wang, H.-G.; Huang, X.-L.; Wang, L.-M.; Zhang, X.-B. Three-Dimensionally Ordered Macroporous FeF_3 and its *In Situ* Homogenous Polymerization Coating for High Energy and Power Density Lithium Ion Batteries. *Energy Environ. Sci.* **2012**, *5*, 8538−8542.

(25) Lou, X. W.; Yuan, C.; Archer, L. A. Shell-by-Shell Synthesis of Tin Oxide Hollow Colloids with Nanoarchitectured Walls: Cavity Size Tuning and Functionalization. *Small* **2007**, *3*, 261−265.

(26) Wang, Z.; Zhou, L.; Lou, X. W. Metal Oxide Hollow Nanostructures for Lithium-Ion Batteries. *Adv. Mater.* **2012**, *24*, 1903−1911.

(27) Xie, Q.; Li, J.; Tian, Q.; Shi, R. Template-Free Synthesis of Zinc Citrate Yolk-Shell Microspheres and Their Transformation to ZnO Yolk-Shell Nanospheres. *J. Mater. Chem.* **2012**, *22*, 13541−13547.

(28) Lai, X.; Li, J.; Korgel, B. A.; Dong, Z.; Li, Z.; Su, F.; Du, J.; Wang, D. Accurate Control of Multishelled Co_3O_4 Hollow Microspheres as High-Performance Anode Materials in Lithium-Ion Batteries. *Angew. Chem., Int. Ed.* **2011**, *50*, 2738−2741.

(29) Zhou, M.; Hu, Y.; Liu, Y.; Yang, W.; Qian, H. Microwave-Assisted Route to Fabricate Coaxial ZnO/C/CdS Nanocables with Enhanced Visible Light-Driven Photocatalytic Activity. *CrystEngComm* **2012**, *14*, 7686−7693.

(30) Li, N.; Jin, S. X.; Liao, Q. Y.; Wang, C. X. ZnO Anchored on Vertically Aligned Graphene: Binder-Free Anode Materials for Lithium-Ion Batteries. *ACS Appl. Mater. Interfaces* **2014**, *6*, 20590−20596.

(31) Wu, M.-S.; Chang, H.-W. Self-Assembly of NiO-Coated ZnO Nanorod Electrodes with Core-Shell Nanostructures as Anode Materials for Rechargeable Lithium-Ion Batteries. *J. Phys. Chem. C* **2013**, *117*, 2590−2599.

(32) Wang, Y.; Jiang, X.; Yang, L.; Jia, N.; Ding, Y. *In Situ* Synthesis of C/Cu/ZnO Porous Hybrids as Anode Materials for Lithium Ion Batteries. *ACS Appl. Mater. Interfaces* **2014**, *6*, 1525−1532.

(33) Huang, X. H.; Wu, J. B.; Lin, Y.; Guo, R. Q.; Zhong, W. W. Ag Decorated Hierarchical Structured ZnO Microspheres and Their Enhanced Electrochemical Performance for Lithium Ion Batteries. *Int. J. Electrochem. Sci.* **2014**, *9*, 6707−6716.

(34) Yu, M.; Shao, D.; Lu, F.; Sun, X.; Sun, H.; Hu, T.; Wang, G.; Sawyer, S.; Qiu, H.; Lian, J. ZnO/Graphene Nanocomposite Fabricated by High Energy Ball Milling with Greatly Enhanced Lithium Storage Capability. *Electrochem. Commun.* **2013**, *34*, 312−315.

(35) Han, F.-D.; Bai, Y.-J.; Liu, R.; Yao, B.; Qi, Y.-X.; Lun, N.; Zhang, J.-X. Template-Free Synthesis of Interconnected Hollow Carbon Nanospheres for High-Performance Anode Material in Lithium-Ion Batteries. *Adv. Energy Mater.* **2011**, *1*, 798−801.

(36) Qiao, L.; Wang, X.; Qiao, L.; Sun, X.; Li, X.; Zheng, Y.; He, D. Single Electrospun Porous NiO-ZnO Hybrid Nanofibers as Anode Materials for Advanced Lithium-Ion Batteries. *Nanoscale* **2013**, *5*, 3037−3042.

(37) Yu, Y.; Gu, L.; Zhu, C.; Tsukimoto, S.; van Aken, P. A.; Maier, J. Reversible Storage of Lithium in Silver-Coated Three-Dimensional Macroporous Silicon. *Adv. Mater.* **2010**, *22*, 2247−2250.

(38) Krajewski, M.; Michalska, M.; Hamankiewicz, B.; Ziolkowska, D.; Korona, K. P.; Jasinski, J. B.; Kaminska, M.; Lipinska, L.; Czerwinski, A. $Li_4Ti_5O_{12}$ Modified with Ag Nanoparticles as an Advanced Anode Material in Lithium-Ion Batteries. *J. Power Sources* **2014**, *245*, 764−771.

(39) Sun, X.; Zhou, C.; Xie, M.; Sun, H.; Hu, T.; Lu, F.; Scott, S. M.; George, S. M.; Lian, J. Synthesis of ZnO Quantum Dot/Graphene Nanocomposites by Atomic Layer Deposition with High Lithium Storage Capacity. *J. Mater. Chem. A* **2014**, *2*, 7319−7326.

(40) Wang, N.; Ma, X.; Xu, H.; Chen, L.; Yue, J.; Niu, F.; Yang, J.; Qian, Y. Porous $ZnMn_2O_4$ Microspheres as a Promising Anode Material for Advanced Lithium-Ion Batteries. *Nano Energy* **2014**, *6*, 193−199.

(41) He, B.-L.; Dong, B.; Li, H.-L. Preparation and Electrochemical Properties of Ag-Modified TiO_2 Nanotube Anode Material for Lithium-Ion Battery. *Electrochem. Commun.* **2007**, *9*, 425−430.

(42) Yan, J.; Song, H.; Yang, S.; Yan, J.; Chen, X. Preparation and Electrochemical Properties of Composites of Carbon Nanotubes Loaded with Ag and TiO_2 Nanoparticle for Use as Anode Material in Lithium-Ion Batteries. *Electrochim. Acta* **2008**, *53*, 6351−6355.

(43) Choi, S. H.; Kang, Y. C. Yolk-Shell, Hollow, and Single-Crystalline $ZnCo_2O_4$ Powders: Preparation Using a Simple One-Pot Process and Application in Lithium-Ion Batteries. *ChemSusChem* **2013**, *6*, 2111−2116.

(44) Yang, K. M.; Hong, Y. J.; Kang, Y. C. Electrochemical Properties of Yolk-Shell-Structured $CuO-Fe_2O_3$ Powders with Various Cu/Fe Molar Ratios Prepared by One-Pot Spray Pyrolysis. *ChemSusChem* **2013**, *6*, 2299−2303.

(45) Sharma, Y.; Sharma, N.; Subba Rao, G. V.; Chowdari, B. V. R. Nanophase $ZnCo_2O_4$ as a High Performance Anode Material for Li-Ion Batteries. *Adv. Funct. Mater.* **2007**, *17*, 2855−2861.

(46) Wang, X.; Qiao, L.; Sun, X.; Li, X.; Hu, D.; Zhang, Q.; He, D. Mesoporous NiO Nanosheet Networks as High Performance Anodes for Li Ion Batteries. *J. Mater. Chem. A* **2013**, *1*, 4173−4176.

(47) Xie, Q.; Ma, Y.; Zeng, D.; Zhang, X.; Wang, L.; Yue, G.; Peng, D.-L. Hierarchical ZnO-Ag-C Composite Porous Microspheres with Superior Electrochemical Properties as Anode Materials for Lithium Ion Batteries. *ACS Appl. Mater. Interfaces* **2014**, *6*, 19895−19904.

(48) Wang, Y.; Li, H.; He, P.; Hosono, E.; Zhou, H. Nano Active Materials for Lithium-Ion Batteries. *Nanoscale* **2010**, *2*, 1294−1305.

(49) Aricò, A. S.; Bruce, P. G.; Scrosati, B.; Tarascon, J.-M.; van Schalkwijc, W. Nanostructured Materials for Advanced Energy Conversion and Storage Devices. *Nat. Mater.* **2005**, *4*, 366−377.

(50) Guo, Y. G.; Hu, J. S.; Wan, L. J. Nanostructured Materials for Electrochemical Energy Conversion and Storage Devices. *Adv. Mater.* **2008**, *20*, 2878−2887.

(51) Hou, L.; Lian, L.; Zhang, L.; Pang, G.; Yuan, C.; Zhang, X. Self-Sacrifice Template Fabrication of Hierarchical Mesoporous Bi-Component-Active $ZnO/ZnFe_2O_4$ Sub-Microcubes as Superior Anode Towards High-Performance Lithium-Ion Battery. *Adv. Funct. Mater.* **2015**, *25*, 238−246.

(52) Choi, S. H.; Kang, Y. C. Using Simple Spray Pyrolysis to Prepare Yolk-Shell-Structured $ZnO-Mn_3O_4$ Systems with the Optimum Composition for Superior Electrochemical Properties. *Chem. - Eur. J.* **2014**, *20*, 1−6.

(53) Shen, X.; Mu, D.; Chen, S.; Wu, B.; Wu, F. Enhanced Electrochemical Performance of ZnO-Loaded/Porous Carbon Composite as Anode Materials for Lithium Ion Batteries. *ACS Appl. Mater. Interfaces* **2013**, *5*, 3118−3125.

(54) Yuan, S.; Huang, X.-L.; Ma, D.-L.; Wang, H.-G.; Meng, F.-Z.; Zhang, X.-B. Engraving Copper Foil to Give Large-Scale Binder-Free Porous CuO Arrays for a High-Performance Sodium-Ion Battery Anode. *Adv. Mater.* **2014**, *26*, 2273−2279.

(55) Taberna, P. L.; Mitra, S.; Poizot, P.; Simon, P.; Tarascon, J.-M. High Rate Capabilities Fe_3O_4-Based Cu Nano-Architectured Electrodes for Lithium-Ion Battery Applications. *Nat. Mater.* **2006**, *5*, 567−573.

(56) Wang, Y.; Zhang, L.; Gao, X.; Mao, L.; Hu, Y.; Lou, X. W. One-Pot Magnetic Field Induced Formation of Fe_3O_4/C Composite Microrods with Enhanced Lithium Storage Capability. *Small* **2014**, *10*, 2815−2819.